Fine study of hierarchical interphase constructed by Ti3SiC2 and carbon nanotubes in SiCf/SiC composites

Yangjun Zou, Xiaozhong Huang, Benhui Fan, Zuojuan Du, Chunqi Wang, Yu Liu, Jianling Yue, Jinbo Bai

Fine study of hierarchical interphase constructed by Ti_3SiC_2 and carbon nanotubes in SiC_f/SiC composites

Yangjun Zou[1,2], Xiaozhong Huang[1,2], Benhui Fan[3], Zuojuan Du[1,2], Chunqi Wang[1,2], Yu Liu[1,2]*, Jianling Yue[1,2]*, Jinbo BAI[4]

1 State Key Laboratory of Powder Metallurgy, Powder Metallurgy Research Institute, Central South University, 410083 Changsha, PR China

2 Hunan Key Laboratory of Advanced Fibers and Composites, Central South University, Changsha, Hunan 410083, PR China

3 Cerema, Research Team ENDSUM, 23 avenue de l'Amiral Chauvin, 49136 Les Ponts de Cé, France

4 LMPS-Laboratoire de Mécanique Paris-Saclay, Université Paris-Saclay, CentraleSupélec, ENS Paris-Saclay, CNRS, Gif-sur-Yvette, France

Corresponding author: Y. Liu (yu_liu@csu.edu.cn), J. Yue (jlyue2010@csu.edu.cn);

Abstract

The interphase in silicon carbide fiber-reinforced silicon carbide ceramic matrix composites (SiC_f/SiC) assumes a significant role in the mechanical properties exhibited at elevated temperatures. The strength, toughness, and chemical stability of a composite is frequently influenced by the optimization of its interphase. In this work, the MAX phase (Ti_3SiC_2) and carbon nanotubes (CNTs) were successively deposited on the SiC_f using the molten salt method and chemical vapor deposition technique, respectively, to create a hierarchical structure. Transmission electron microscopy was employed to undertake a comprehensive investigation of the interfacial component in SiC_f/SiC composites. The detailed study of interphases in SiC_f/SiC composites has been conducted through the analysis of crystallization, the

bonding natures, and the micromorphology, encompassing geometry and constituent characteristics. A bilayer consisting of TiC-Ti_3SiC_2/Ti_5Si_3 and a vertical array of carbon nanotubes (CNTs) with a length of 7 μm is fabricated on the surface of SiC_f/Ti_3SiC_2-CNTs. The SiC_f/Ti_3SiC_2/SiC and SiC_f/Ti_3SiC_2-CNTs/SiC composites exhibit lamellar structures of Ti_3SiC_2, which indicates a further crystallization of Ti_3SiC_2 resulting from the formation of SiC matrix by PIP procedure. The interphase of SiC_f/Ti_3SiC_2-CNTs/SiC composite may be categorized into four distinct layers: a TiC phase, a $TiSi_2$ phase, a transition phase of $TiSi_2$/TiC, and a Ti_3SiC_2 phase. This interphase structure is more intricate compared to the interphase structure observed in the SiC_f/Ti_3SiC_2/SiC composite. This research indicates significant value for the future design and optimization of interfaces.

Keywords: Ti_3SiC_2, Carbon nanotubes, SiC_f/SiC composites, Interface structure

1. Introduction

Silicon carbide fiber-reinforced silicon carbide ceramic matrix (SiC_f/SiC) composites have garnered significant interest because of their exceptional mechanical qualities, thermal conductivity, and semiconductor characteristics.[1-3] These aforementioned accomplishments serve as evidence of the potential utilization of SiC_f/SiC in several high-technology industries, including aerospace manufacturing, electric systems, electronic circuits, nuclear energy systems, etc.[4-6] However, the SiC_f/SiC ceramic matrix composite is brittle due to its defect-sensitive characteristics, which fails to meet the mechanical demands in industrial applications. Thus, enhancing the strength and toughness of SiC_f/SiC is a fundamental requirement for its practical utilization. The interface with relative low strength will undergo dissociation

upon transmission of matrix cracks to the interface. The crack deviates from the intrinsic direction of expansion, and the extension of the crack expansion path promotes stress release, enhancing the strength and toughness of the ceramic matrix composite material. Therefore, a qualitative characterization of the interface between fibers and matrix can help us to find a solution to improve the strength and toughness of the composite materials.[7-9]

Extensive research efforts have been dedicated to investigating the interphase in the SiC_f/SiC composites.[10-12] The pursuit of enhanced performances has led to a significant focus on the interphase, which involves the utilization of innovative materials and hierarchical microstructures.[13, 14] The utilization of ternary layered carbide MAX phase synthesized by a molten salt method serves as an illustrative instance of innovative materials. The MAX phase exhibits a multi-layered structure with different electron density distributions, which can possess the MAX phase with both metallic and ceramic properties through the manipulation of its microstructures.[15] Li Mian et al has documented that the utilization of the MAX phase as a buffer interface can effectively deflect cracks in the interphase by absorbing a substantial quantity of fracture energy within the fiber-reinforced composites.[16, 17] In contrast to PyC and BN, the MAX phase exhibits superior binding strength with SiC, which enhances the efficiency of load transfer efficiency.[18-22] In our previous work, we have additionally documented the utilization of the MAX phase materials in the enhancement of electromagnetic wave absorption in SiC composites.[23] Therefore, the MAX phase can be seen as a flexible interface that facilitates the enhancement of both strength and toughness in fiber-reinforced ceramic matrix composites.

Extensive research has been conducted on the synthesis of one-dimensional (1D)

nanomaterials with exceptional mechanical properties on the interface as buffer coatings, such as carbon nanotubes (CNTs) and silicon nitride (Si_3N_4) nanowires. These studies aim to enhance the toughness and pre-fabricated body structure of the SiC_f/SiC composites.[24, 25] Nevertheless, achieving uniform dispersion of 1D nanomaterials with high aspect ratios in the composites, like CNTs, poses a challenge due to the entanglement and coalescence resulting from van der Waals forces.[26] The utilization of a core-shell structure or multi-coating is a more versatile approach to attaining mechanical reinforcement.[27, 28] A quantitative characterization of the interfaces of the multi-coating in the interphase of SiC_f/SiC composites presents an intriguing area of investigation in this particular situation.

This study investigates the hierarchical interface formed by the combination of MAX phase and CNTs in SiC_f/SiC composites. The composites were fabricated by the controlled molten salt method and chemical vapor deposition (CVD) technique. The analysis of the composites' crystalline structures and bonding characteristics was based on X-ray diffraction (XRD) and X-ray photoelectron spectroscopy (XPS). To preserve the integrity of the interface and minimize the detrimental effects of cutting, the samples intended for cross-section characterization were meticulously prepared by focus ion beam (FIB) technique in a scanning electron microscope (SEM). Subsequently, the micromorphology of the samples was examined using high-resolution transmission electron microscopy **(**HR-TEM).

2. Experimental section

2.1. Materials

SiC_f (Cansas 3303) was supplied by Xinli New Material Co., Ltd. Titanium powders (Ti, 325 mesh) were supplied by Beijing Licheng Innovation Metal Materials

Technology Co., Ltd. Sodium chloride (NaCl) and potassium chloride (KCl) powder, Xylene (C_8H_{10}), ferrocene ($C_{10}H_{10}Fe$) were bought from Sinopharm Chemical Reagent Co., Ltd. Polycarbosilane (PCS) was bought from Hunan Boxiang New Material Co. LTD. Hydrogen (H_2), Acetylene (C_2H_2), Argon (Ar) with a purity of 99.99% were bought from Changsha Gaoke Gas Co. LTD.

2.2. Materials preparation

The molten salt synthesis (MSS) method was used to introduce Ti_3SiC_2 on the surface of SiC_f.[29] First, the mixture powder of NaCl, KCl, and Ti with the molar ratio of NaCl: KCl: Ti = 4:4:1 was grounded in an alumina crucible. Then, SiC_f bundles were evenly buried in the mixture powder. The molten salt reaction was carried out by placing the alumina crucible in an argon-gas-protected tube furnace and heating it to 1000°C at a rate of 5°C/min for 1 hour. Afterward, the reaction temperature was quenched to 500 ^oC and then cooled naturally. When the furnace was cooled down to room temperature, the reaction products were taken out and washed several times with deionized water for removing residual salts. The obtained sample was named as SiC_f/Ti_3SiC_2.

Floating catalytic chemical vapor deposition (CVD) was used to grow carbon nanotubes (CNTs) on SiC_f/Ti_3SiC_2.[23] SiC_f/Ti_3SiC_2 was placed in a tube furnace in a gas mixture of argon, hydrogen, and acetylene with a volume ratio of 400:90:10. The temperature of CVD was 700 °C with an increasing rate of 10 °C/min. The catalyst used in the CVD was a xylene/ferrocene solution with a concentration of ferrocene of 0.5 g/mL. After 10 minutes of reaction, the sample was removed and cooled down to room temperature naturally. The obtained sample was named as SiC_f/Ti_3SiC_2-CNTs.

The precursor impregnation and pyrolysis (PIP) method was used to prepare the SiC_f/SiC composite.[30] The SiC_f before and after treatment were placed in liquid PCS and vacuum-impregnated for 16 h. Then, the impregnated SiC_f was pyrolyzed for 2 h at 1100°C under an argon atmosphere in a high-temperature tube furnace. The impregnation and pyrolysis processes were repeated several times until the increased weight of the composite was less than 1%. The schematic diagram of SiC_f/Ti_3SiC_2-CNTs/SiC composites in three steps is illustrated in Fig. 1.

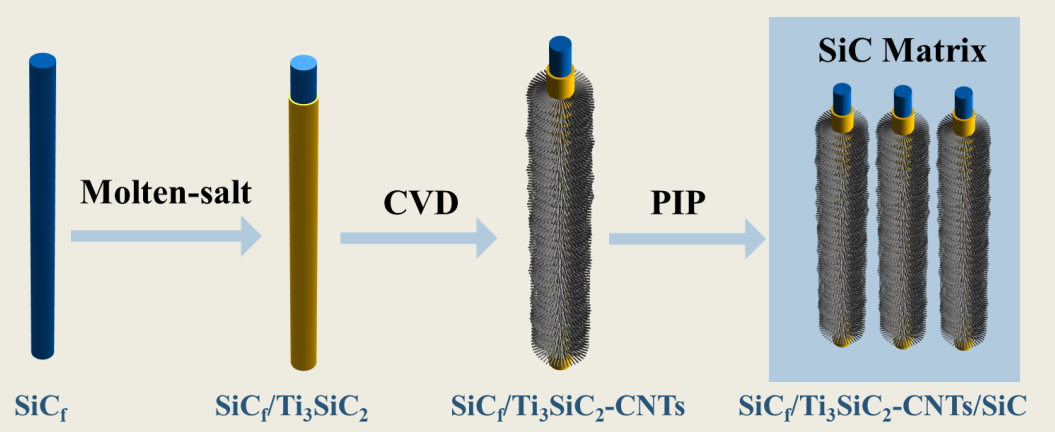

Fig. 1 The schematic diagram of the synthesis process of SiC_f/Ti_3SiC_2-CNTs/SiC composites

2.3. Characterization

The crystalline phases of raw SiC_f and SiC_f/Ti_3SiC_2 were characterized by an X-ray diffractometer (XRD) (Rigaku SmartLab SE, Japan) with a Cu target Kα ray. The scanning range of 2θ was from 10° to 80° with a step of 10°/min. The X-ray photoelectron spectra of the SiC fibers after molten-salt synthesis were measured using an X-ray photoelectron spectrometer (XPS; PHI 5000 Versaprobe III). The morphology and microstructure of the samples were observed by a scanning electron microscope (SEM) (Tescan Mira4) at 10 kV. The TEM samples were cut by focused ion beams (FIB, Nova NanoSEM230), which was described in detail elsewhere.[31]

TEM imaging was performed by a Talos F200 with a field emission gun (XFEG) operating at an accelerating voltage of 200 kV. Energy-dispersion X-ray microscopy (EDX) was carried out on the same equipment and operated at 200 kV in a STEM mode. The EDX mapping was acquired for 10 min.

3. Results and discussion

3.1. The microstructure of SiC_f/Ti_3SiC_2 and SiC_f/Ti_3SiC_2-CNTs

Fig. 2a displays X-ray diffraction (XRD) patterns of the original SiC fiber (SiC_f) and the resultant SiC fiber coated with Ti_3SiC_2 (SiC_f/Ti_3SiC_2). The original state of SiC_f consists predominantly of a β phase, as evidenced by the presence of three distinct peaks at 2θ = 35.6, 60, and 71.8°. These peaks can be attributed to (111), (220), and (311) crystallographic planes of β-SiC (JCPDS no.29-1129), respectively. At an angle of 2θ = 26°, a broad and shapeless halo is observed, attributed to the presence of unbound carbon in SiC fibers. After the molten salt reaction, the SiC_f/Ti_3SiC_2 sample exhibited distinct peaks corresponding to the Ti_3SiC_2 and TiC phases, along with the immediate phases of Ti_5Si_3 phases. The observed peaks at 2θ= 39.7°, 41.1, 42.7, and 60.4 are corresponding to the crystal structure planes (104), (008), (105), and (110) of Ti_3SiC_2 (JCPDS no. 40-1132), respectively. These peaks provide evidence of a successful deposition of Ti_3SiC_2 onto the SiC_f substrate.[32] The X-ray photoelectron spectroscopy (XPS) spectra presented in Fig. 2b provides evidence of the existence of C, Ti, Si, and O components in SiC_f/Ti_3SiC_2 material, thereby indicating the surface binding state of this composite. The Ti 2p spectra have characteristic peaks at 453.8 Ev, 458.6 eV, and 464.3eV, corresponding to the Ti-Si and Ti-O interactions.[33] Upon analyzing the Si 2p spectra, it is observed that two distinct peaks can be discerned. The first peak, denoted as Si-C, is located at a binding

energy of 98.1 eV. The second peak corresponds to Si-O and is observed at a binding energy of 102 eV. The signal at 281.3 eV in C 1s spectra supports the presence of C-Ti bonds in Ti_3SiC_2.[34]

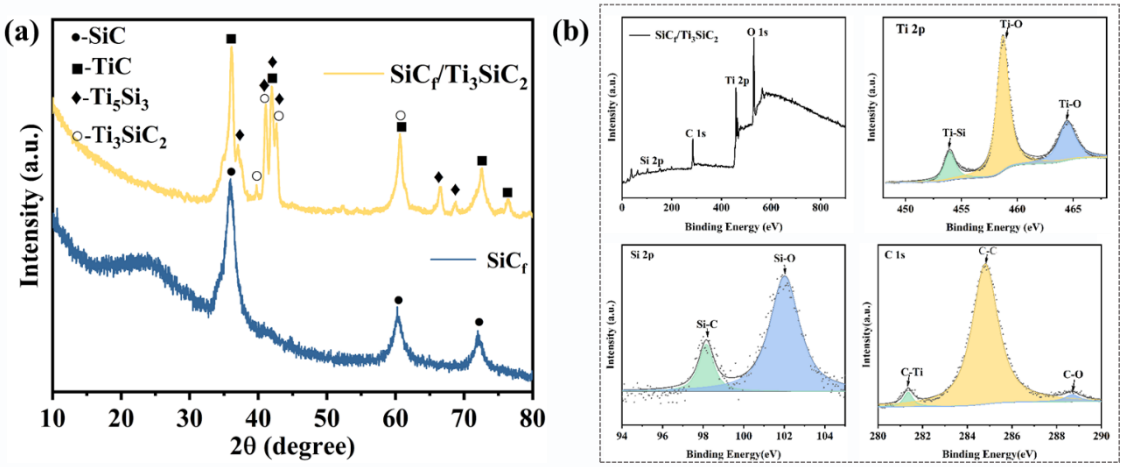

Fig. 2 (a) XRD patterns of raw SiC_f and SiC_f/Ti_3SiC_2, (b) XPS patterns of SiC_f/Ti_3SiC_2.

Fig. 3a-b illustrates the cross-sectional morphology of SiC_f after undergoing molten salt treatment. The SiC_f material is coated by a continuous layer with a thickness of 1.25 nm. This material has a bi-layer structure characterized by a gradient distribution of crystalline grains. The central layer has a thickness of 0.33 nm, whereas one of the peripheral layers has a thickness of 0.92 nm (Fig. 3b). The layer demonstrates few fractures and micropores, which confers advantageous for subsequent synthesis SiC_f/SiC composites.

To provide additional validation for the bi-layer structure of the interphase, a longitudinal section of the interphase on SiC_f is obtained by focused ion beam (FIB) extraction. The FIB sample is depicted in Fig. 3c. Fig. 3d-e displays the SEM morphologies of the sample prepared by FIB. The bilayer of the interphase with dense adhesion can be observed on the SiC_f material. Furthermore, it has been observed that the interphase can be divided into three regions, denoted as f, g, and h arranged in

ascending order from the bottom to the top. To validate the microstructure in each specific region, TEM with energy-dispersive X-ray spectroscopy (EDS) is employed to examine the composition, as depicted in Fig. 3f-k and outlined in Table 1.

As shown in Fig. 3i-k and Table 1, area f is primarily comprised of Si (52%) and C (46%), with a negligible amount of Ti (0.15%). Its HRTEM image exhibits a polycrystalline structure characterized by a grain plane spacing of 0.25 nm. This spacing corresponds to the (111) crystalline planes of β-SiC grains. The electron diffraction rings inside Fig. 3f are attributed to the crystalline grains of β-SiC. Differently from area f, the elemental composition in area g is with Ti of 47% and C of 48%, with a minor presence of Si (2.67%). This composition suggests that the layer primarily comprises the titanium carbide (TiC) phase. The inner layer TiC on the SiC_f shows columnar crystal morphology. The area h exhibits two distinct crystal structures, as depicted in Fig. $3h_1$-h_2. Fig. $3h_1$ displays a crystal face spacing of 0.23 nm in the grains, while the crystal face spacing of the polycrystalline diffraction rings is 0.23 nm and 0.26 nm, respectively. This observation infers the presence of the Ti_3SiC_2 phase. The crystal plane spacing in Fig. $3h_2$ is 0.2 nm, indicating the (202) crystal plane of the Ti_5Si_3 phase. In addition, as listed in Table 1, the composition of the area h is with Ti of 49%, Si of 34%, and C of 14%. This composition with the elemental ratios agrees with the compounds Ti_3SiC_2 and Ti_5Si_3. Hence, the SiC_f/Ti_3SiC_2 composites demonstrate a bilayer structure comprising an internal phase of TiC and an external amalgamation of Ti_3SiC_2 and Ti_5Si_3.

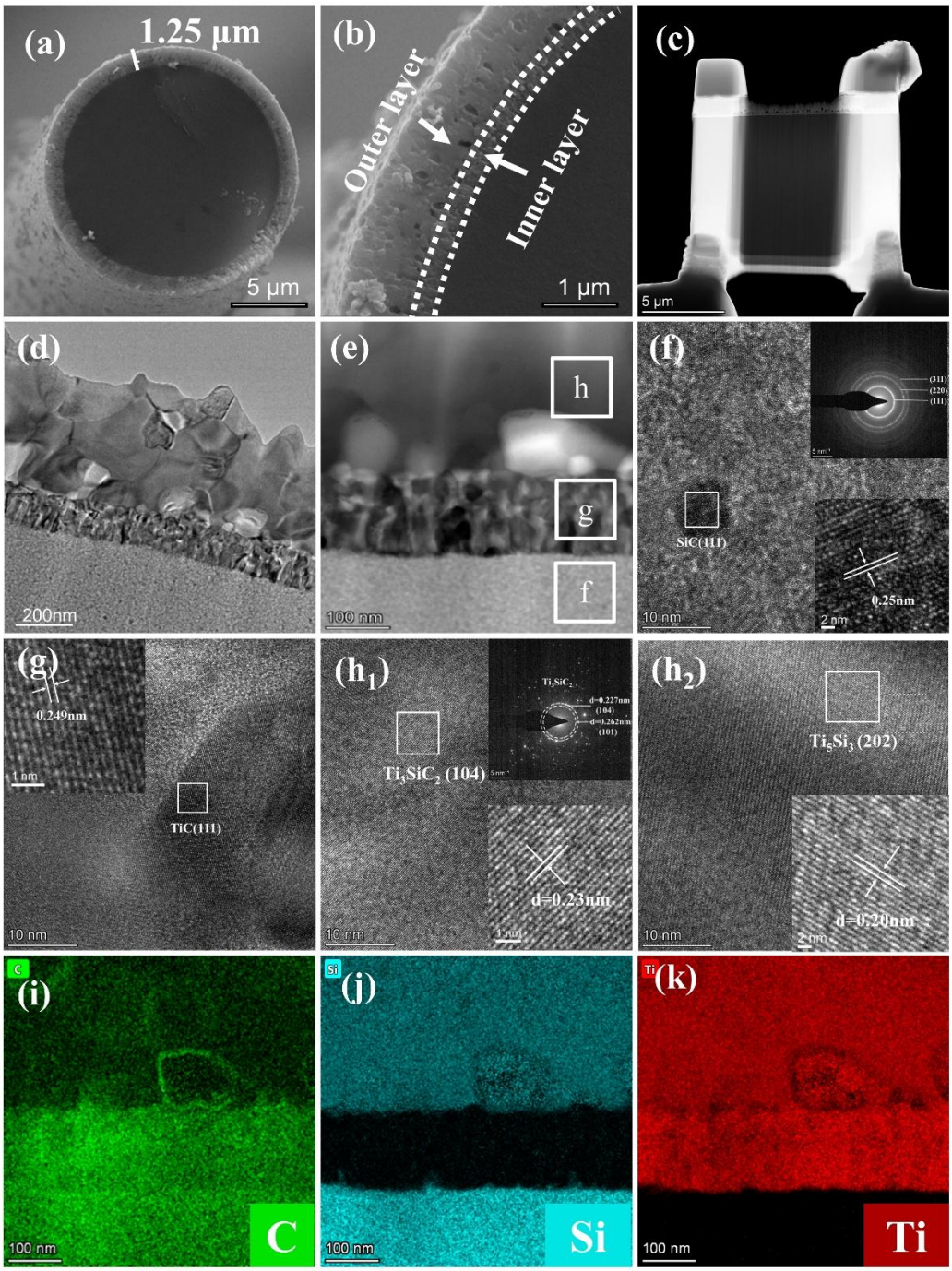

Fig. 3 The SEM images (a-c), TEM images (d-h) and EDS elemental mapping (i-k) images of SiC_f/Ti_3SiC_2.

Table 1 The elemental composition of three areas in Fig. 3e from EDS.

Area	Atom Fraction/%			Phase
	Ti	Si	C	

f	0.15	51.82	45.96	SiC
g	46.92	2.67	47.52	TiC
h	49.55	33.91	13.65	Ti_3SiC_2, Ti_5Si_3

Fig. 4 depicts the morphological characteristics of SiC_f/Ti_3SiC_2-CNTs obtained by CVD. The SiC fiber bundle exhibits a homogeneous distribution of CNTs, forming a porous network with a thickness of 7μm. This network comprises numerous radial nano-arrays, effectively partitioning the spacious region surrounding the fiber bundle into smaller compartments. Importantly, this arrangement does not impede the ingress of reactive gases into the inner region of the fiber bundle. CNTs can be observed within the tiny pores of the SiC_f bundle. The structural composition of the Ti_3SiC_2 phase has been preserved in its bilayer after the deposition of CNTs, as depicted in Fig. 4d.

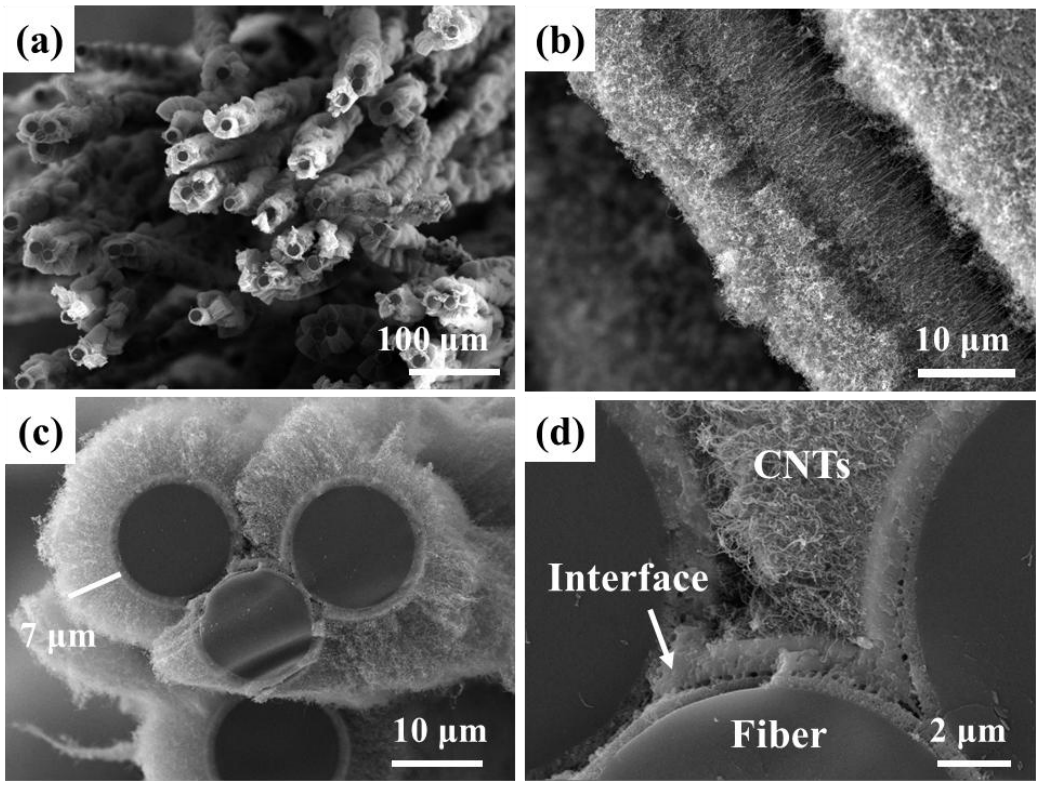

Fig. 4 SEM images of SiC_f/Ti_3SiC_2-CNTs

3.2. The interphase structure of $SiC_f/Ti_3SiC_2/SiC$ composites

Fig. 5 illustrates the SEM morphologies of $SiC_f/Ti_3SiC_2/SiC$ composites. As depicted in Fig. 5a, a SiC matrix is consistently enveloping on the SiC_f/Ti_3SiC_2. The cracks and defects can be detected between the matrix and fibers, which are induced by the volume shrinkage following the pyrolysis process. It is possible to mitigate the density of cracks by increasing the cycle numbers of PIP, but the complete elimination of cracks is hard to achieve. Fig. 5b illustrates the morphology of the interphase, where the Ti_3SiC_2 layer is uniformly dispersed on the SiC_f substrate, serving as a protective barrier. Furthermore, the bilayer structure of the Ti_3SiC_2 phase remains stable in the composites after the following PIP treatments. The interphase components depicted in Fig. 5c-d does not have obvious pores between SiC and SiC_f, which infers a significant degree of wettability. Furthermore, it's worth noting that the lamellar structure of Ti_3SiC_2 is present in the outer layer. However, this particular lamellar structure is not observed in Fig. 3, which implies that the pyrolysis process promotes the formation of Ti_3SiC_2.

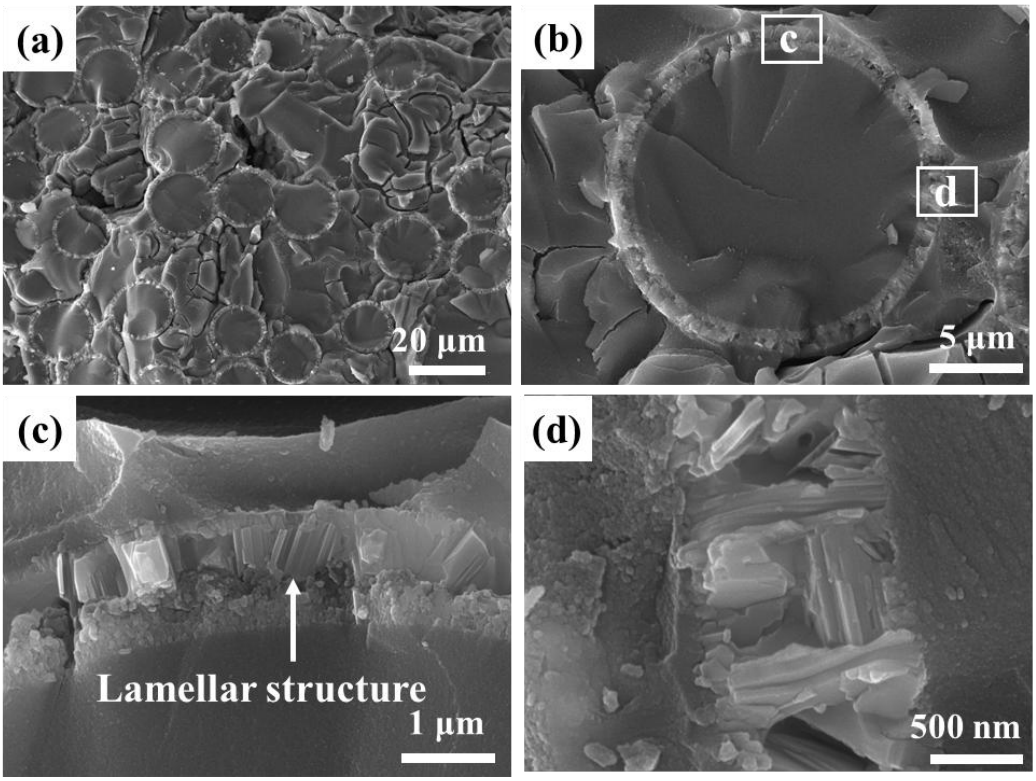

Fig. 5 SEM images of $SiC_f/Ti_3SiC_2/SiC$ composites

Fig. 6a-b depicts backscatter electron (BSE) images of the cross-section view of the $SiC_f/Ti_3SiC_2/SiC$ composite after careful polishing. The average thickness of the interphase between the SiC matrix and SiC_f/Ti_3SiC_2 is found to be 1μm. This microstructure of the interphase is further characterized by TEM. Fig. 6d displays the high-magnification image of the FIB slice, showing four unique zones labeled as i, j, k, and l. Fig. 6e-h, i-l, and Table 2 present the results of EDS mapping, HRTEM images, and the element fractions of Ti, C, Si, and O elements in the four zones. According to EDS analysis, zones i and l predominantly consist of C and Si elements, representing SiC fibers and SiC matrix, respectively. Zone j is predominantly composed of Ti (53.02%) and C (30.28%) elements, representing the inner layer of TiC in the bilayer structure. Zone k is mostly comprised of Ti (45.98%), Si (13.81%), and C (25.09%) elements. These elemental compositions agree with the composition of Ti_3SiC_2. According to the findings depicted in Fig. 6i and l, it can be observed that

zone i and l consisted of polycrystalline phases, characterized by the presence of numerous finely dispersed SiC grains. The selected electron diffraction images inside Fig. 6i and l exhibit three distinct diffraction rings, which can be attributed to the crystal planes of (111), (220), and (311) of β-SiC grains. The SED image of zone j exhibits diffraction rings that indicate polycrystalline TiC. The morphology of HR-TEM in Fig. 6j reveals their crystal plane spacings of 0.21 nm and 0.24 nm, which can be attributed to the (200) and (111) crystal planes of TiC grains (JCPDS no. #32-1383), respectively. Fig. 6k displays an HRTEM image and selected electron diffraction, which indicates a single-crystal phase of Ti_3SiC_2 in the k region. In conclusion, the interphase architecture of $SiC_f/Ti_3SiC_2/SiC$ composites consists of a polycrystalline phase of TiC and a monocrystalline phase of Ti_3SiC_2.

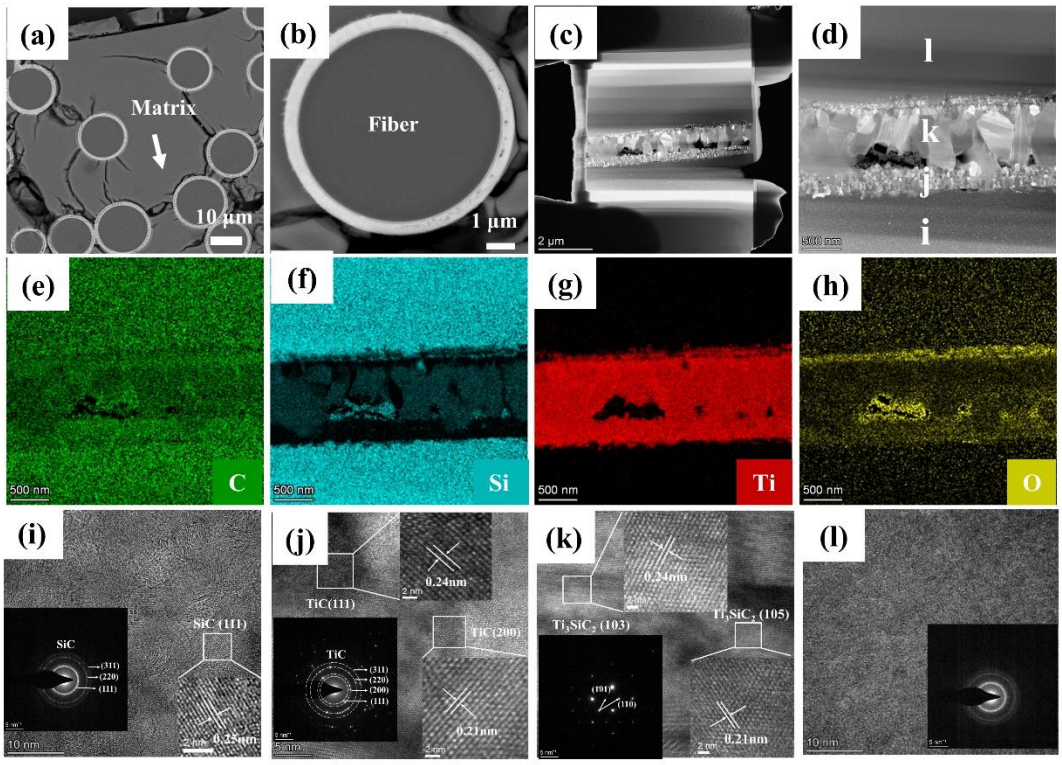

Fig. 6 SEM images (a-c) and TEM images (d-l) of $SiC_f/Ti_3SiC_2/SiC$ composites

Table 2 The elemental composition of four areas in Fig. 6d from EDS.

Region	Atom Fraction/%	Phase

	Ti	Si	C	
i	0.16	51.57	37.34	SiC
j	53.02	1.77	30.28	TiC
k	45.98	13.81	25.09	Ti_3SiC_2
l	0.23	53.58	35.29	SiC

3.3. Microstructure of SiC_f/Ti_3SiC_2-CNTs/SiC composites

Fig. 7 illustrates the morphologies of SiC_f/Ti_3SiC_2-CNTs/SiC composites. As depicted in Fig. 7a, during the PIP method, the SiC matrix is simultaneously deposited on the silicon carbide fibers and CNTs. Nevertheless, it can be observed from Fig. 7c that the density of the network of CNTs gradually decreases from the interior to the outside of the fiber surface. Consequently, the CNTs closing to the fiber surface experience more rapid densification, which forms a SiC sheath layer. However, due to the limited effective reactive area and the significant amount of free space, the carbon nanowires far away from the fiber surface do not achieve complete densification. This leads to the formation of dendritic structures composed of SiC rods, as depicted in Fig. 7b.

As depicted in Fig. 7a, the surface of SiC_f/SiC exhibits a high density. However, the internal densification is relatively low, resulting in the presence of numerous holes of varying sizes. Additionally, CNTs are randomly oriented on the micrometer-sized SiC rods. Nevertheless, the effective filling of pores between these SiC rods has not been achieved. The problem might be attributed to the excessive density of carbon nanowires within the prefabricated SiC_f/SiC composites, as well as the rapid densification of the material's surface layer during the PIP process. This early formation of a "crust" hinders sufficient reactive penetration of the matrix.

Furthermore, Fig. 7c infers that the interfacial layer has a persistent bilayer structure. Upon examination under magnification, as seen in Fig. 7d, it is observed that the outer layer likewise exhibits a characteristic lamellar structure consistent with that of Ti_3SiC_2.

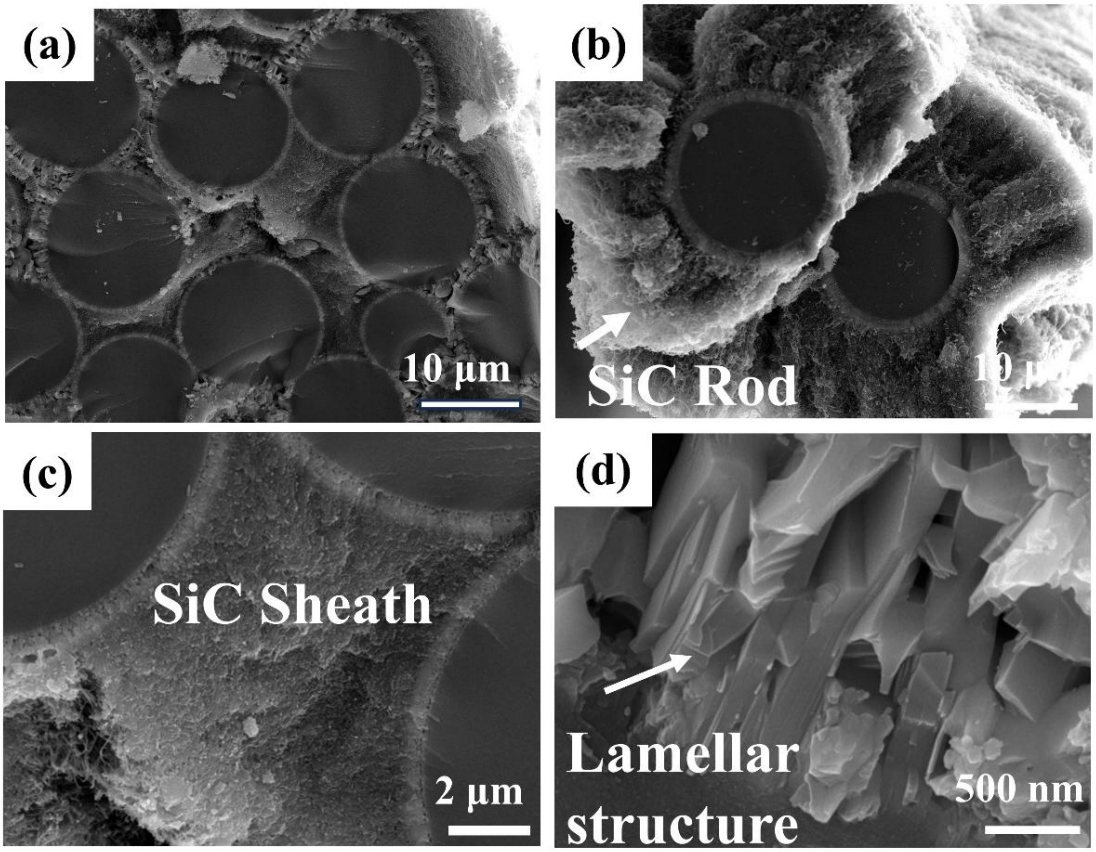

Fig. 7 SEM morphologies of the SiC_f/Ti_3SiC_2-CNTs/SiC composites

Fig. 8a shows the SEM image of the SiC_f/Ti_3SiC_2-CNTs/SiC composite protected by resin after finely polishing. The modified fibers, interphases, and SiC matrix can be effectively characterized, and the dispersion of CNTs remains uniform without degradation during the SiC sintering. The fibers exhibit independence from one other and do not achieve full densification.

The TEM morphology of SiC_f/Ti_3SiC_2-CNTs/SiC composites prepared by FIB is shown in Fig. 8b. Based on the EDS element distribution diagram, the composite can be divided into six distinct zones, as visually depicted in Fig. 8c, e-h. In Fig. 8d, zone

6 is depicted as being expanded, revealing the presence of several curved CNTs that are dispersed inside the SiC matrix. Based on the elemental fractions of Ti, Si, and C as presented in Table 3, it may be inferred that zone 1 corresponds to the SiC_f phase. Zone 2 mostly consists of Ti and C, with a limited presence of Si elements. This composition suggests that the primary phase in this zone is TiC. The interplanar distance of the grain surface spacing is measured to be 0.25 nm, corresponding to TiC (111) crystallographic plane, as observed in HRTEM morphology in Fig. 8i. Zone 3 exhibits a substantial concentration of Ti and Si while demonstrating a relatively low presence of carbon. According to Fig. 8j, the grain plane spacing in this region is 0.25 nm, agreeing with the (111) plane of $TiSi_2$ (JCPDS no.10-0225). The Si element starts to diminish in zone 4, signifying the presence of a transition phase consisting of $TiSi_2$ and TiC. According to Fig. 8k, the grain surface spacing in Zone 5 is 0.24 nm. This spacing corresponds to the (103) plan of Ti_3SiC_2 (JCPDS no.40-1132). In zone 6, the amount of C is comparatively greater than that observed in other zones due to the presence of CNTs. Additionally, it's worth noting that certain Fe particles can also be observed in zone 6 as depicted in Fig. 8l. These particles are introduced into the system through the catalyst in CVD. The interphase observed in the SiC_f/Ti_3SiC_2-CNTs/SiC composite exhibits greater complexity compared to that of SiC_f/Ti_3SiC_2/SiC. Especially, the formation of a $TiSi_2$ phase in zone 3 and a transition phase of $TiSi_2$/TiC phase in zone 4, which are not detected in the SiC_f/Ti_3SiC_2/SiC composite.

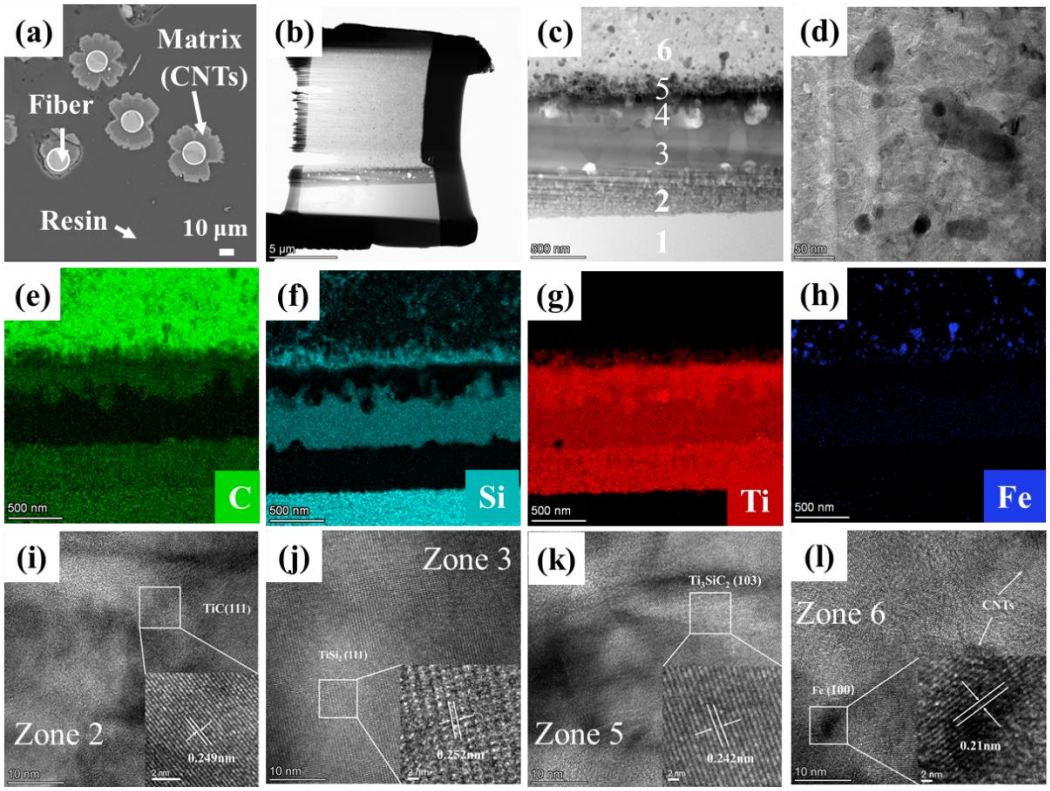

Fig. 8 SEM (a-b) and TEM images (c-l) of SiC_f/Ti_3SiC_2-CNTs/SiC composites

Table 3 The elemental composition of six areas in Fig. 8c from EDS.

Area	Atom Fraction/%					Phase
	Ti	Si	C	O	Fe	
1	0.16	59.25	38.22	-	-	SiC
2	55.01	1.62	31.30	8.70	0.11	TiC
3	52.93	34.38	3.83	3.69	1.26	$TiSi_2$
4	67.62	6.53	19.01	3.50	0.42	$TiSi_2$/TiC
5	20.40	30.93	33.05	9.15	4.43	Ti_3SiC_2
6	0.15	3.71	89.27	5.66	0.03	C, SiC

4. Conclusion

This research provides a comprehensive investigation including the synthesis of MAX phase coatings and the characterization of the microstructure of the modified

SiC_f/SiC composites. The purpose of this study is to evaluate microstructural differences of interphases between SiC_f/Ti_3SiC_2/SiC and SiC_f/Ti_3SiC_2-CNTs/SiC composites. The findings can be briefly described in the following manner: (1) After molten-salt synthesis, a unique bilayer structure manifests on SiC_f, wherein the inner layer consists of TiC while the outer layer comprises Ti_3SiC_2 and Ti_5Si_3. (2) Following the CVD process, a CNTs vertical array with an average thickness of 7 μm can be formed on the SiC_f/Ti_3SiC_2 substrate. (3) The presence of the lamellar structures of Ti_3SiC_2 has been seen in the SiC_f/Ti_3SiC_2/SiC and SiC_f/Ti_3SiC_2-CNTs/SiC composites, but not in either SiC_f/Ti_3SiC_2 or SiC_f/Ti_3SiC_2-CNTs, which infers a further crystallization of Ti_3SiC_2 through PIP process for adding SiC matrix. (4) The interphase observed in the SiC_f/Ti_3SiC_2-CNTs/SiC composite is found to be more intricate compared to that of SiC_f/Ti_3SiC_2/SiC. Especially, the creation of a $TiSi_2$ phase and a transition phase of the $TiSi_2$/TiC phase is identified in the former composite, but these phases are not recognized in the latter one. This study presented a case study for analyzing the interphase region consisting of MAX phase and CNTs in SiC_f-reinforced ceramic composites.

Declaration of Competing Interest

The authors declare that they have no known competing financial interests or personal relationships that could have appeared to influence the work reported in this paper.

Acknowledgment

This work is supported by the National Natural Science Foundation of China (Grant No. 52002403), the Natural Science Foundation of Hunan province (Grant No.

2022JJ40607)，and the key project of Changsha (Grant No. kh2103011).

Reference

[1] P. Wang, F. Liu, H. Wang, H. Li, and Y. Gou, A review of third generation SiC fibers and SiCf/SiC composites. Journal of Materials Science & Technology. **35**(12) (2019) 2743-2750.

[2] G. Liu, X. Zhang, J. Yang, and G. Qiao, Recent advances in joining of SiC-based materials (monolithic SiC and SiCf/SiC composites): Joining processes, joint strength, and interfacial behavior. Journal of Advanced Ceramics. **8**(1) (2019) 19-38.

[3] H. Liu, L. Li, J. Yang, Y. Zhou, Y. Ai, Z. Qi, Y. Gao, and J. Jiao, Characterization and Modeling Damage and Fracture of Prepreg-MI SiC/SiC Composites under Tensile Loading at Room Temperature. Applied Composite Materials. **29**(3) (2022) 1167-1193.

[4] L. Zhou, T. Yang, Z. Fang, J. Zhou, Y. Zheng, C. Guo, L. Zhu, E. Wang, X. Hou, K.-C. Chou, and Z.L. Wang, Boosting of water splitting using the chemical energy simultaneously harvested from light, kinetic energy and electrical energy using N doped 4H-SiC nanohole arrays. Nano Energy. **104**((2022).

[5] S. Liu, T. Yang, E. Wang, H. Wang, Z. Du, S. Cao, Q. Zhang, K.-C. Chou, and X. Hou, Ultra-stable and bifunctional free-standing SiC photoelectrocatalyst for water remediation. Journal of Cleaner Production. **396**((2023).

[6] L. Song, F. Zhang, Y. Chen, L. Guan, Y. Zhu, M. Chen, H. Wang, B.R. Putra, R. Zhang, and B. Fan, Multifunctional SiC@SiO2 Nanofiber Aerogel with Ultrabroadband Electromagnetic Wave Absorption. Nano-Micro Letters. **14**(1) (2022).

[7] H.J. Yu, X.G. Zhou, W. Zhang, H.X. Peng, C.R. Zhang, and Z.L. Huang, Mechanical properties of 3D KD-I SiCf/SiC composites with engineered fibre–matrix

interfaces. Composites Science and Technology. **71**(5) (2011) 699-704.

[8] J. Gao, Y. Bai, H. Fan, G. Song, X. Zou, Y. Zheng, and X. He, Phase- field simulation of microscale crack propagation/deflection in SiCf/SiC composites with weak interphase. Journal of the American Ceramic Society. **106**(8) (2023) 4877-4890.

[9] A. Nöth, J. Maier, K. Schönfeld, and H. Klemm, Wet chemical deposition of BN, SiC and Si3N4 interphases on SiC fibers. Journal of the European Ceramic Society. **41**(5) (2021) 2988-2994.

[10] J. Sun, W. Liu, X. Lv, and J. Jiao, Characterization of BN interface and its effect on the mechanical behavior of SiCf/SiC composites. Vacuum. **211**((2023).

[11] H. Yang, X. Zhou, W. Shi, J. Wang, P. Li, F. Chen, Q. Deng, J. Lee, Y.-H. Han, F. Huang, L. He, S. Du, and Q. Huang, Thickness-dependent phase evolution and bonding strength of SiC ceramics joints with active Ti interlayer. Journal of the European Ceramic Society. **37**(4) (2017) 1233-1241.

[12] R.R. Naslain, The design of the fibre-matrix interfacial zone in ceramic matrix composites. Composites Part A: Applied Science and Manufacturing. **29**(9-10) (1998) 1145-1155.

[13] J. Yang, F. Ye, and L. Cheng, In-situ formation of Ti3SiC2 interphase in SiCf/SiC composites by molten salt synthesis. Journal of the European Ceramic Society. **42**(4) (2022) 1197-1207.

[14] R.R. Naslain, R.J.F. Pailler, and J.L. Lamon, Single- and Multilayered Interphases in SiC/SiC Composites Exposed to Severe Environmental Conditions: An Overview. International Journal of Applied Ceramic Technology. **7**(3) (2009) 263-275.

[15] Z. Zhang, X. Duan, D. Jia, Y. Zhou, and S. van der Zwaag, On the formation mechanisms and properties of MAX phases: A review. Journal of the European

Ceramic Society. **41**(7) (2021) 3851-3878.

[16] M. Li, K. Wang, J. Wang, D. Long, Y. Liang, L. He, F. Huang, S. Du, and Q. Huang, Preparation of TiC/Ti2AlC coating on carbon fiber and investigation of the oxidation resistance properties. Journal of the American Ceramic Society. **101**(11) (2018) 5269-5280.

[17] M. Li, F. Chen, X. Si, J. Wang, S. Du, and Q. Huang, Copper–SiC whiskers composites with interface optimized by Ti3SiC2. Journal of Materials Science. **53**(13) (2018) 9806-9815.

[18] S. Haji Amiri, M. Ghassemi Kakroudi, T. Rabizadeh, and M. Shahedi Asl, Characterization of hot-pressed Ti3SiC2–SiC composites. International Journal of Refractory Metals and Hard Materials. **90**((2020).

[19] C.B. Spencer, J.M. Córdoba, N.H. Obando, M. Radovic, M. Odén, L. Hultman, and M.W. Barsoum, The Reactivity of Ti2AlC and Ti3SiC2 with SiC Fibers and Powders up to Temperatures of 1550°C. Journal of the American Ceramic Society. **94**(6) (2011) 1737-1743.

[20] H.G. Lee, D. Kim, J.Y. Park, and W.J. Kim, Formation of Ti3SiC2interphase coating on SiCf/SiC composite by electrophoretic deposition. International Journal of Applied Ceramic Technology. **15**(3) (2017) 602-610.

[21] B. Yang, X. Zhou, and Y. Chai, Mechanical properties of SiCf/SiC composites with PyC and the BN interface. Ceramics International. **41**(5) (2015) 7185-7190.

[22] Z. Lu, Z. Qi, J. Yang, H. Liu, and J. Jiao, The wetting- to- nonwetting transition of CVD BN coatings deposited at different temperatures. International Journal of Applied Ceramic Technology. (2023).

[23] Y. Zou, X. Huang, B. Fan, Z. Tang, J. Zhou, P. Peng, X. Liu, J. Zhu, Y. Liu, and J. Yue, Constructing hierarchical Ti3SiC2 layer and carbon nanotubes on SiC fibers

for enhanced electromagnetic wave absorption. Ceramics International. **49**(5) (2023) 8048-8057.

[24] L. Feng, K. Li, Z. Zhao, H. Li, L. Zhang, J. Lu, and Q. Song, Three-dimensional carbon/carbon composites with vertically aligned carbon nanotubes: Providing direct and indirect reinforcements to the pyrocarbon matrix. Materials & Design. **92**((2016) 120-128.

[25] W. Feng, L. Zhang, Y. Liu, X. Li, L. Cheng, and H. Bai, Fabrication of SiCf-CNTs/SiC composites with high thermal conductivity by vacuum filtration combined with CVI. Materials Science and Engineering: A. **662**((2016) 506-510.

[26] Z. Li, X. Li, B. Zhang, X. Zhou, C. Liu, Y. Jiang, C. Zhen, C. Zheng, L. Zhang, and L. Cheng, Enhanced thermal and mechanical properties of optimized SiCf/SiC composites with in-situ CNTs on PyC interface. Ceramics International. **46**(11) (2020) 18071-18078.

[27] K. Sun, J. Yu, C. Zhang, and X. Zhou, In situ growth carbon nanotube reinforced SiCf/SiC composite. Materials Letters. **66**(1) (2012) 92-95.

[28] S. Zhao, X. Zhou, J. Yu, and P. Mummery, Mechanical properties and in situ crack growth observation of SiC/SiC composites. Ceramics International. **40**(5) (2014) 7481-7485.

[29] B. Chahhou, C. Labrugère-Sarroste, F. Ibalot, J. Danet, and J. Roger, Synthesis of Ti3SiC2 coatings onto SiC monoliths from molten salts. Journal of the European Ceramic Society. **42**(13) (2022) 5484-5492.

[30] S. Zhao, X. Zhou, J. Yu, and P. Mummery, Effect of heat treatment on microstructure and mechanical properties of PIP-SiC/SiC composites. Materials Science and Engineering: A. **559**((2013) 808-811.

[31] Y. Liu, A.L. Hamon, P. Haghi-Ashtiani, T. Reiss, B. Fan, D. He, and J. Bai,

Quantitative Study of Interface/Interphase in Epoxy/Graphene-Based Nanocomposites by Combining STEM and EELS. ACS Appl Mater Interfaces. **8**(49) (2016) 34151-34158.

[32] F. Zhang, L. Zhao, G. Yu, J. Chen, S. Yan, J. He, and F. Yin, Effect of annealing temperature on microstructure and mechanical properties of plasma sprayed TiC-Ti5Si3-Ti3SiC2 composite coatings. Surface and Coatings Technology. **422**((2021).

[33] Z. Zhong, B. Zhang, J. Ye, Y. Ren, and F. Ye, Tailorable microwave absorption properties of macro-porous core@shell structured SiC@Ti3SiC2 via molten salt shielded synthesis (MS3) method in air. Journal of Alloys and Compounds. **927**((2022).

[34] R. Kang, Z. Zhang, L. Guo, J. Cui, Y. Chen, X. Hou, B. Wang, C.T. Lin, N. Jiang, and J. Yu, Enhanced Thermal Conductivity of Epoxy Composites Filled with 2D Transition Metal Carbides (MXenes) with Ultralow Loading. Sci Rep. **9**(1) (2019) 9135.